

Solidification Structure of Coating Layer in Hot-dip Zn-11% Al-3% Mg-0.2% Si-coated Steel Sheet and Phase Diagram of the System

Wataru YAMADA*
Koki TANAKA
Kohsaku USHIODA

Kazuhiko HONDA
Hidetoshi HATANAKA

Abstract

The solidification structure of the coating layer in hot-dip Zn-11%Al-3%Mg-0.2%Si coated steel sheet was studied by metallographic examinations together with the calculation of a phase diagram based on Thermo-Calc. The observation exhibited that the solidification structure is a combination of the Zn/Al/MgZn₂ ternary eutectic structure, the primary fcc-Al phase and the MgZn₂ phase, which is different from the predicted one under an equilibrium state in the sense that meta-stable MgZn₂ instead of stable Mg₂Zn₁₁ was observed under the present condition. Excluding the Mg₂Zn₁₁ phase from the equilibrium phase diagram, the metastable phase diagram was calculated and excellent agreement was obtained between the calculation and the experiment in terms of the solidification structure of the coating layer. The small amount of Ti addition to the coating bath was confirmed to lead to the formation of fine dendrite structure. Detailed EBSD observation revealed that TiAl₃ acts as heterogeneous nucleation sites of the primary fcc-Al.

1. Introduction

The alloy phase diagram is a design map that provides guidelines on the optimum alloy composition and process conditions to obtain the desired microstructure in materials design. Thus, it plays an extremely important role in the development of materials. With a focus on calculation of phase diagrams (CALPHAD), since the late 1980s, Nippon Steel Corporation has introduced thermodynamic equilibrium analysis software and thermodynamic databases, such as SOLGASMIX and Thermo-Calc,^{1,2)} and applied them to analyze

practical materials and actual processes.³⁾ The most important merit of CALPHAD is that it permits a sufficiently accurate estimation of the phase diagram of a multicomponent system from the thermodynamic data of two- and three-component systems using a solution model that reflects the alloy phase physical structure, whereas the phase diagram of many practical materials is difficult to determine experimentally because they are multicomponent systems containing four or more components. Another benefit of CALPHAD is that it permits easy decision of the metastable equilibrium phase diagram, which is difficult to observe experimentally.

* General Manager, Mathematical Science & Technology Research Lab., Advanced Technology Research Laboratories 20-1, Shintomi, Futtu, Chiba 293-8511

In this report, we present an example in which CALPHAD was fully utilized to analyze the solidification structure of a hot-dip alloy-coating layer with good corrosion resistance.

In recent years, a hot-dip Zn-Al-Mg-coated steel sheet with a Zn-Al coating layer with Mg added to enhance the corrosion resistance has been increasingly used.⁴⁻⁷⁾ Since the hot-dip Zn-Al-Mg coating layer is a multicomponent system, its solidification structure is more complicated than that of the hot-dip Zn-Al coating layer. It has been known that the types of phases and the homogeneity and size of the microstructure of the coating layer of galvanized coating steel sheet significantly influence the basic properties of the steel sheet, such as corrosion resistance, formability, and appearance.^{5, 8)} Therefore, it is important to understand the solidification structures in the coating layer and grasp their influence on various properties of the coating steel sheet. For understanding the solidification process of hot-dip Zn-Al-Mg coating, we observed the solidification structures and studied the solidification path using the CALPHAD technique.

On the other hand, many Zn-Al and Zn-Al-Mg alloys used for hot-dip Zn-Al-coated steel and hot-dipped Zn-Al-Mg-coated steel sheets form a dendrite of the fcc-Al phase (hereinafter abbreviated as the Al phase) as the primary phase. Since the size of the primary-phase dendrite depends on the cooling rate, it is considered possible to refine the crystals by varying the degree of undercooling. It is known that to refine the crystals of an aluminum alloy for forging, the inoculation effect produced by the addition of TiAl₃, TiB₂, or TiC particles is effective.⁹⁾ In hot-dip zinc coating with Al added also, the microstructure refinement effect with Ti-based precipitates as inoculant nuclei can be expected since the primary phase is an Al phase. However, it has not been studied in earnest. In the present study, we added Ti to the coating bath for hot-dip Zn-11% Al-3% Mg-0.2 Si-coating and studied the influence of the formed Al phase on the crystal refinement and the crystal refinement mechanisms.

2. Experimental Procedure and Phase Diagram Calculation Method

The coated steel sheet used for the evaluation of the solidification structure was prepared by employing the hot-dip galvanizing simulator shown in Fig. 1. First, a 0.8-mm-thick steel sheet was heated to 1,053 K in an N₂ atmosphere containing 3 vol% H₂ and main-

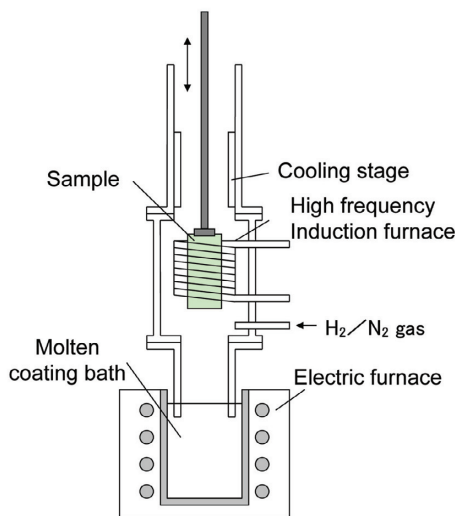


Fig. 1 Schematic view of galvanizing simulator

tained at that temperature for 60 s to reduce the sheet surface. After the steel sheet was cooled to 773 K at the same atmosphere, it was dipped in a 723 K coating bath for 3 s, with the coating weight controlled from 70 to 90 g/m² each side by N₂ wiping, and then cooled down at a rate of 10°C/s. The coating bath composition was Zn-11 mass%Al-3 mass%Mg-0.2 mass%Si. The solidification structure of the coating layer was observed using a field-emission scanning electron microscope (FE-SEM). In addition, the solidification phases were subjected to an elementary analysis using an electron probe microanalyzer (EPMA). The individual phases of the solidification structure were identified by X-ray diffraction (XRD).

The coated steel sheet with Ti added was prepared by a method similar to that described above, except that 100 ppm Ti was added to the coating bath. The solidification structure of the coating layer was observed by a method similar to that described above. After that, a grain orientation analysis was conducted by employing the electron backscattering diffraction pattern (EBSD) technique to evaluate the crystal conformation between the inoculant nucleus and primary phase.

The calculation of phase diagrams was carried out by use of Thermo-Calc,²⁾ where the thermodynamic parameters of ternary (Al-Mg-Zn) alloy phases described by sub-lattice model¹⁰⁾ were substituted from those obtained by Liang et al.¹¹⁾ Since the purpose of our phase diagram calculation was to study the main coating structures, the added trace element, Si, was not considered.

3. Solidification Structure of Zn-11 mass% Al-3 mass% Mg-0.2 mass% Si Coating Layer

Fig. 2 shows the calculated equilibrium phase diagram of a Zn-Al-Mg ternary system with Mg fixed at 3 mass%, and Fig. 3 shows the calculated changes in type and amount of the precipitate phases in the equilibrium solidification process. It can be seen from the two figures that a ternary peritectic-eutectic reaction—liquid phase L + MgZn₂ → Mg₂Zn₁₁ + Al phase—occurs at 623 K and that a ternary eutectic reaction—L → Zn phase + Al phase + Mg₂Zn₁₁—takes place at 616 K, where “Zn phase” is an abbreviation of the hcp-Zn phase. It is expected that when the 11% Al coating being studied solidifies in the equilibrium state, the Al phase will decompose after the above ternary peritectic-eutectic reaction and ultimately three phases—the

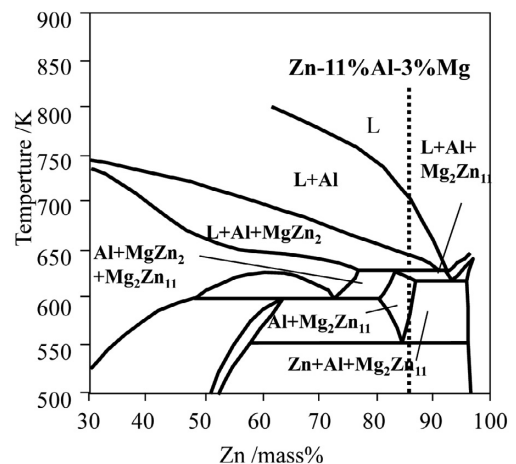


Fig. 2 Calculated equilibrium phase diagram of the Zn-Al-Mg system at 3mass%Mg

Zn phase, Al phase, and Mg_2Zn_{11} phase—will be observed.

Fig. 4 shows the results of an EPMA observation of a cross section of the coating layer. As solidification structures, a Zn-prevalent eutectic structure, an Al-prevalent structure and a Mg-prevalent structure were observed. On the basis of the knowledge obtained from the equilibrium phase diagrams shown in Figs. 2 and 3, we considered that the Zn-prevalent eutectic structure appearing lamellar in the SE image was a ternary peritectic-eutectic structure containing Mg_2Zn_{11} , that the Al-prevalent structure was an Al phase formed as the primary phase, and that the Mg-prevalent structure was a Zn-Mg based intermetallic compound. However, from the XRD results of the coating layer shown in Fig. 5, the only intermetallic compound detected was $MgZn_2$, and the presence of Mg_2Zn_{11} could not be confirmed. From this, it may be considered that in the actual solidification process, a ternary eutectic reaction of Al, Zn, and $MgZn_2$, not the above peritectic-eutectic reaction predicted from the equilibrium phase diagrams, was occurring.

Figs. 6 and 7 show the calculated metastable phase diagrams with the crystallization of Mg_2Zn_{11} neglected (suspended) in the calcu-

tions. Fig. 8 shows the liquidus temperature diagram of a Zn-Al-Mg ternary system obtained in the metastable equilibrium calculation and the calculated solidification path for a Zn-11%Al-3%Mg alloy. From these phase diagrams, the solidification of a Zn-11 mass%Al-3 mass%Mg alloy begins with the formation of an Al phase as the

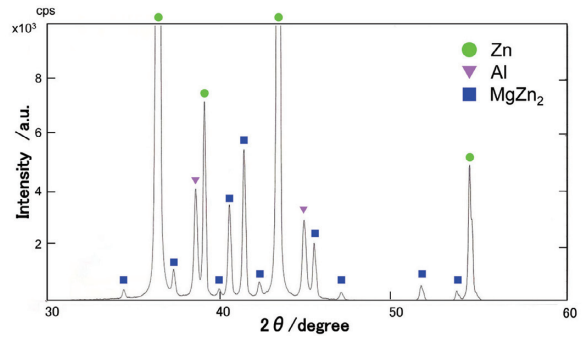


Fig. 5 X-ray diffraction patterns of Zn-11%Al-3%Mg-0.2%Si coating

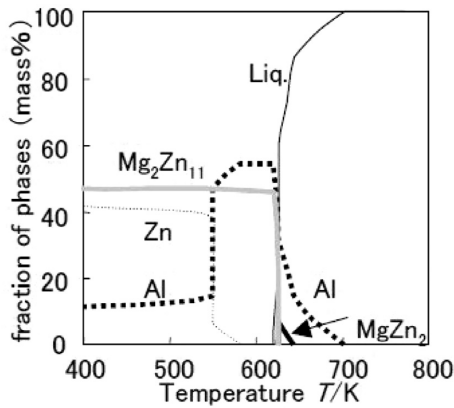


Fig. 3 Calculated change in kind and quantity of phases in Zn-11mass%Al-3mass%Mg alloy in the course of equilibrium solidification

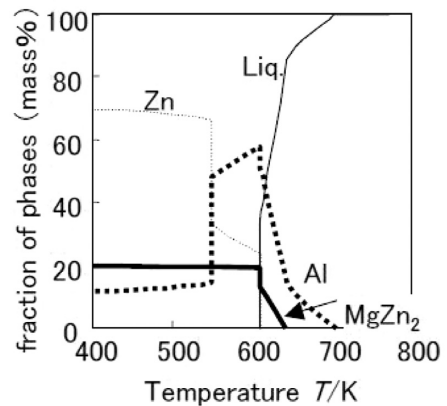


Fig. 6 Calculated change in kind and quantity of phases in Zn-11mass%Al-3mass%Mg alloy in the course of metastable solidification

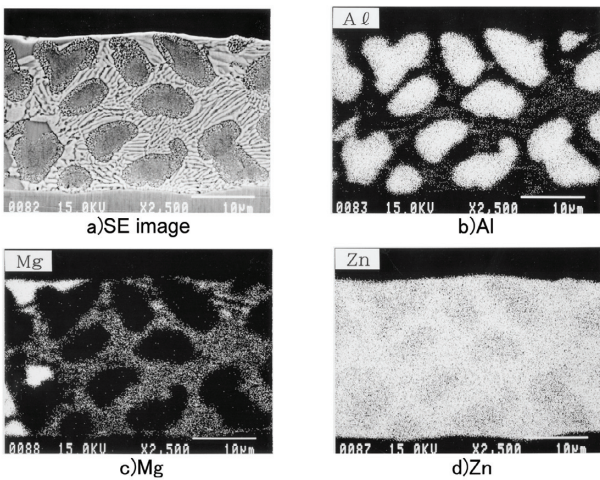


Fig. 4 Cross sectional SEM and EDX images of coating layer in Zn-11%Al-3%Mg-0.2%Si coating
a) SE image, b) Al, c) Mg, d) Zn

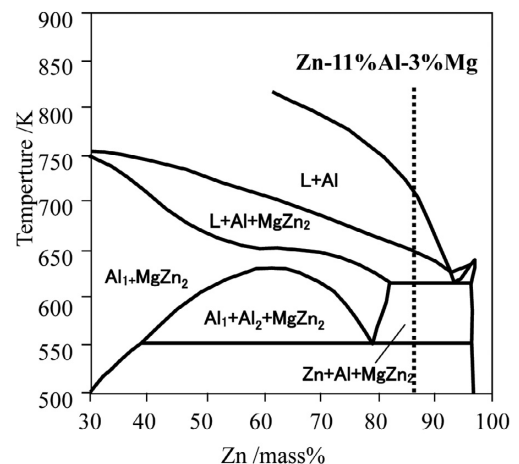


Fig. 7 Calculated meta-stable phase diagram of the Zn-Al-Mg system at 3mass%Mg

primary phase, through eutectic crystallization of the Al phase and $MgZn_2$, and ends in the ternary eutectic crystallization of the Al phase, Zn phase, and $MgZn_2$ phase. Thus, the calculated solidification structure coincides with the actual solidification structure. The eutectic temperature of the ternary Zn phase/Al phase/ $MgZn_2$ system in the metastable state is 609 K, which is not significantly different from the ternary peritectic-eutectic temperature in the equilibrium state shown in Fig. 2 (623 K) or the Zn phase/Al phase/ $MgZn_2$ eutectic temperature (616 K).

The crystal structure of $MgZn_2$ is a Type C14 Laves structure. This structure is similar to that of the Frank-Kasper phase.^{12, 13)} Since coordination 12, which is the local structure of the liquid phase, has a high degree of short-range regularity, the nucleation energy barrier in the liquid phase is considered small.¹⁴⁾ Generally, coating layers solidify rapidly (10^3 C/s in the present experiment). Therefore, it is considered that the ternary eutectic reaction of the Zn phase/Al phase/ $MgZn_2$ occurred preferentially because of the rapid $MgZn_2$ nucleation under high-degree undercooling.

Fig. 9 shows the results of FE-SEM observations of the ternary

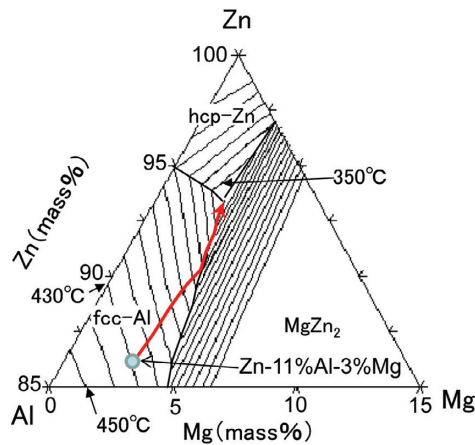


Fig. 8 Calculated solidification path of Zn-11mass%Al-3mass%Mg alloy

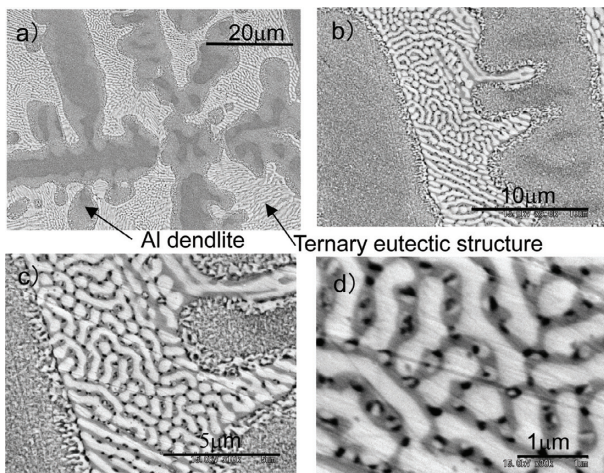


Fig. 9 SEM images of ternary eutectic structure and Al dendrite in Zn-11%Al-3%Mg-0.2%Si coating
a), b) Low magnification micrograph and c), d) High magnification micrograph

eutectic structure and the primary Al phase. The high-magnification micrograph of the ternary eutectic structure (Fig. 9(d)) reveals a lamellar structure consisting of three phases. It is considered that the white phase corresponds to a Zn phase, the gray phase to an $MgZn_2$ phase, and the black phase to an Al phase. The ternary eutectic structure shown in Fig. 9(d) can be observed as a solidification structure in which a Zn and $MgZn_2$ phases grew in the form of lamellae, and then, in that $MgZn_2$ phase, a mixture of a fine Zn and Al phases are rod shaped. As shown in Fig. 9(c), at the interface between the primary Al phase and ternary eutectic structure also, the separation to the Zn and Al phases was observed. It is considered that those Al and Zn phases surrounding them are the primary Al and the Al-rich Al phases and Zn phases precipitated from the Al phase contained in the ternary eutectic structure by monotectic reaction.

4. Solidification Structure When Ti Was Added

Even when Ti was added, the types of phases of the solidification layer and the proportions of precipitation of the individual phases were similar to those when Ti was not added. However, as shown in Fig. 10(b), the marked refining of the primary Al phase in the form of an equiaxed dendrite was observed. It is already known that the addition of $TiAl_3$ particles, TiB_2 particles or TiC particles to refine the grain size of an aluminum alloy for forging is effective.⁹⁾ It has been clarified that in the refinement of grains of the Al phase formed in the hot-dip zinc coating with Al added, the same effect can be obtained by adding Ti. The results of an EPMA observation of the coating layer obtained are shown in Fig. 11. It can be seen that a Ti-Al based intermetallic compound ($TiAl_3$) exists in the center of the Al phase dendrite. It was conjectured that the $TiAl_3$ served as the inoculation nucleus to refine the primary Al phase. Therefore, we studied the crystal conformation and orientation relationship between the inoculation nucleus ($TiAl_3$) and the crystallized Al phase.

Fig. 12 shows the EBSD mapping images of the primary Al and Zn phases forming a ternary eutectic structure of the coating layer

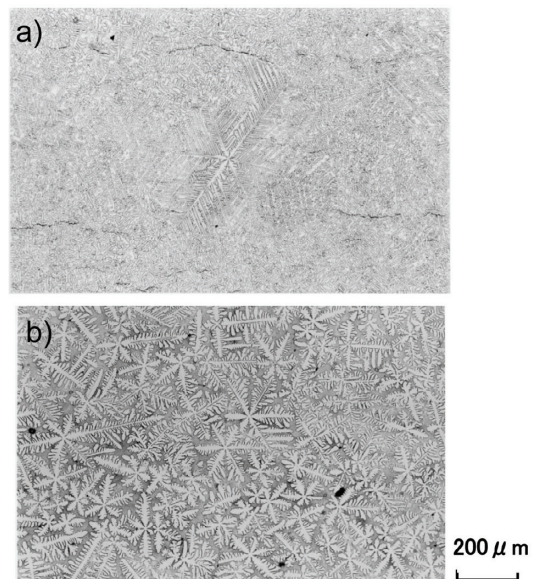


Fig. 10 Optical micrographs showing dendrite structures at the top surface
a) Without Ti addition and b) with Ti addition

with Ti added. As shown in the Al phase orientation-mapping image, the Al phase dendrite spread in four directions when the ground face was {001}, whereas it spread in six directions when the ground face was {111}. Although Al is a face-centered cube, the primary Al phase contains 40% Zn. It is already known that when the Zn content is reasonably high, the orientation of preferential growth of dendrite changes from $\langle 100 \rangle$ to $\langle 110 \rangle$ ¹⁵⁾. When a crystal structure whose dendrite has grown in the $\langle 110 \rangle$ orientation is observed from the {001} ({111}) side, the dendrite of the solidification structure is seen as a structure that has grown in four (six) directions.

In the orientation-mapping image of Al shown in Fig. 12, each individual dendrite shows only one grain orientation regardless of its location. The primary Al phase that has solidified at a high temperature is separated into two phases—Al and Zn phases—by the monotectic reaction at low temperatures. This shows that the grain orientation of the Al phase after the monotectic reaction retains the information about the grain orientation of the primary Al phase. Therefore, it can be seen that the orientation-mapping image of Al shown in Fig. 12 represents the solidification structure of the primary Al

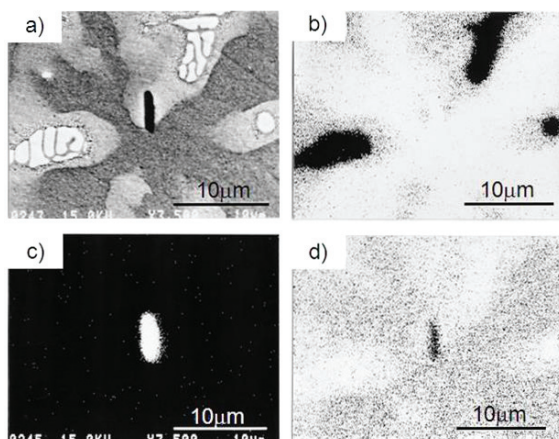


Fig. 11 X-ray images by EPMA showing the Ti-Al intermetallic compound in the center of the Al dendrite in Zn-11%Al-3%Mg-0.2%Si coating with 100 mass ppm Ti addition
a) SE image, b) Al, c) Ti and d) Zn

phase observed from various directions at a time.

The results of the EBSD observation of the nucleation sites and their surroundings, taken from the {001} side of the Al phase, are shown in Fig. 13. The EBSD pattern of intermetallic compounds that are nucleation sites agrees well with that of the TiAl_3 crystal prepared separately. The grain orientation of the ground face of the TiAl_3 indexed using the above result was the {100} side, as shown in Fig. 13 (d). Next, the EBSD pole figures of the Al phase and TiAl_3 , and the crystal models obtained from them are shown in Fig. 13 (f)-(i). The grain orientations of the Al phase and TiAl_3 were all parallel not only at the ground face, but also the planes perpendicular to the {100} side. Therefore, it can be seen that the grain orientations of TiAl_3 in the center of the dendrite and those of the Al phase around the TiAl_3 completely coincide with each other three-dimensionally. From the crystal model of the Al phase shown in Fig. 13 (g), it can be confirmed that the dendrite of the Al phase shown in Fig. 13 (a) has grown in the $\langle 110 \rangle$ direction.

The Al phase has an fcc structure, and TiAl_3 has a D0_{22} structure. The D0_{22} structure consists of two layers of the Al unit lattice (fcc) with the Al at the four corners and the center replaced with Ti. Table 1 shows the planar discrepancy, δ , between the Al and TiAl_3 phases at each of the representative index planes calculated from the lattice constant in accordance with the procedure employed by Ohashi et al.¹⁶⁾ According to the EBSD measurement results shown in Fig. 13, there was a perfectly coherent orientation relationship between the TiAl_3 in the center and the Al phase surrounding it. This shows that the Al phase dendrite grew epitaxially from TiAl_3 at the center. The reason for this is considered to be as follows. Since the Al phase has a similar unit lattice to TiAl_3 and all the index planes making up the unit lattice show good coherence, as shown in Table 1, TiAl_3 crystals are converted into an Al phase of the fcc structure simply by replacing Ti with Al and the resultant Al phase can easily grow epitaxially.

From the above results, the Al phase in the coating layer was refined when Ti was dissolved in the hot-dip Zn-11 mass%Al-3 mass%Mg-0.2 mass%Si coating bath because it is supposed that TiAl_3 crystallized before the Al phase in the coating and acted as Al nucleation sites. In other words, it is considered that the heterogeneous nucleation of the Al phase occurred on the TiAl_3 surface, lowering the degree of undercooling required for nucleation, and as a result, a fine, equiaxed solidification structure was obtained.

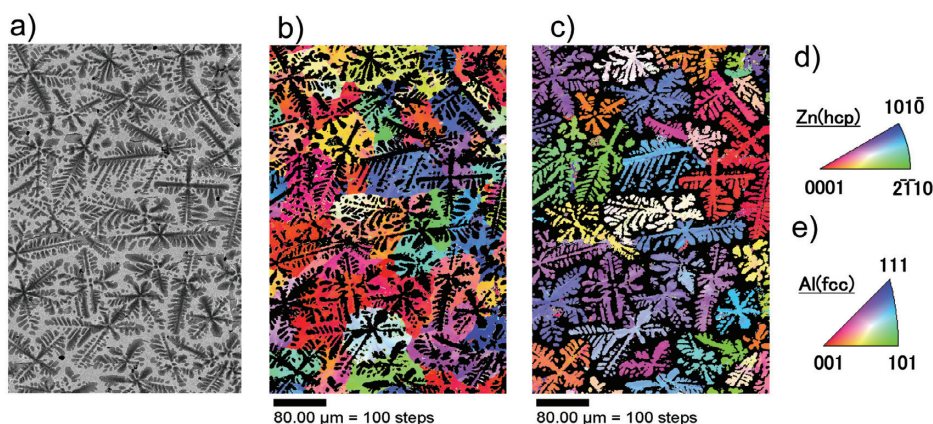


Fig. 12 BSE image and EBSD orientation mapping, showing the solidified structure of Zn-11%Al-3%Mg-0.2%Si coating with 100 mass ppm Ti addition
a) BSE image, b) Orientation mapping image of Zn, c) Orientation mapping image of Al, d) Stereo triangles of Zn (hcp) and e) Al (fcc) showing color-indicated orientation

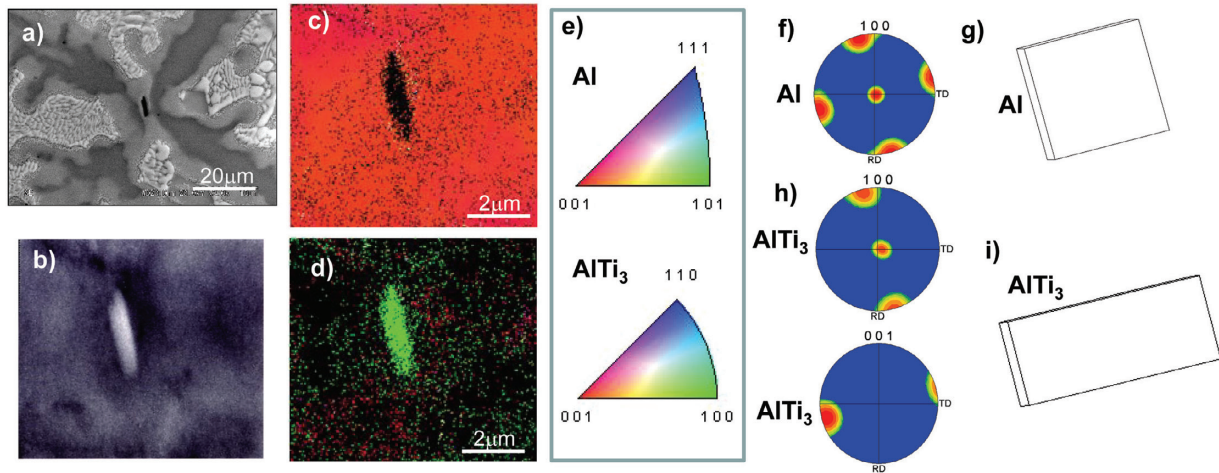


Fig. 13 BSE image and EBSD orientation mapping showing $TiAl_3$ in Al dendrite
 a) BSE image of Al dendrite, b) Enlarged BSE image of a), c) Orientation mapping of Al, d) Orientation mapping of $TiAl_3$, e) Stereo triangles of Al (fcc) and $TiAl_3$ (tetragonal), f) {100} pole figure of Al dendrite, g) Crystal orientation of Al dendrite, h) {100} pole figure and {001} pole figure of $TiAl_3$ and i) Crystal orientation of $TiAl_3$

Table 1 Planar registry between $TiAl_3$ and Al

Plane form	$[uvw]_s$	$[uvw]_n$	$d [uvw]_s$	$d [uvw]_n$	θ_1 (deg)	$\delta \frac{(hkl)_s}{(hkl)_n}$
$(001)_{TiAl_3} // (001)_{Al}$	$[100]_{TiAl_3}$	$[100]_{Al}$	3.854	4.049	0	4.8
	$[110]_{TiAl_3}$	$[110]_{Al}$	2.725	2.862	0	
	$[010]_{TiAl_3}$	$[010]_{Al}$	3.854	4.049	0	
$(100)_{TiAl_3} // (100)_{Al}$	$[010]_{TiAl_3}$	$[010]_{Al}$	3.854	4.049	0	3.6
	$[021]_{TiAl_3}$	$[011]_{Al}$	2.868	2.862	2.8	
	$[001]_{TiAl_3}$	$[001]_{Al}$	8.584	4.049	0	
$(102)_{TiAl_3} // (101)_{Al}$	$[\bar{2}01]_{TiAl_3}$	$[\bar{1}01]_{Al}$	2.868	2.862	0	2.2
	$[\bar{2}21]_{TiAl_3}$	$[\bar{1}11]_{Al}$	2.301	2.338	1.5	
	$[010]_{TiAl_3}$	$[010]_{Al}$	3.854	4.049	0	
$(110)_{TiAl_3} // (110)_{Al}$	$[\bar{1}10]_{TiAl_3}$	$[\bar{1}10]_{Al}$	2.725	2.862	0	4.2
	$[\bar{2}21]_{TiAl_3}$	$[\bar{1}11]_{Al}$	2.301	2.338	2.6	
	$[001]_{TiAl_3}$	$[001]_{Al}$	8.584	4.049	0	

$d[uvw]_s, d[uvw]_n$: Atomic displacement along $[uvw]_s$ and $[uvw]_n$, respectively θ_1 : Difference in angle between $[uvw]_s$ and $[uvw]_n$

5. Conclusion

We conducted a detailed study of the solidification structure of the hot-dip Zn-11 mass%Al-3 mass%Mg-0.2 mass%Si coating layer whose cooling rate is relatively high. As a result, it was found that the solidification structure was in a metastable state with Mg_2Zn_{11} suspended and that the solidification was completed by the ternary eutectic reaction, $L \rightarrow Zn$ phase + Al phase + $MgZn_2$, without any accompanying crystallization of Mg_2Zn_{11} . In a coating layer inoculated with Ti, the heterogeneous nucleation of primary Al phase with $TiAl_3$ as the nucleation site occurred, producing a markedly refined structure. A detailed EBSD orientation analysis revealed that the grain orientation of $TiAl_3$ as the nucleation site completely coincided three-dimensionally with that of the Al phase around $TiAl_3$, indicating that the Al phase grew epitaxially on the $TiAl_3$ during solidification.

References

- 1) Eriksson, G.: *Chemica Scripta*. 8, 1072 (1975)
- 2) Sundman, B.: *CALPHAD*. 9, 153 (1985)
- 3) Yamada, W., Matsumiya, T.: *Shinnittetsu Gihō*. (342), 38 (1991)
- 4) Komatsu, A. et al.: *Tetsu-to-Hagané*. 86, 534 (2000)
- 5) Tsujimura, T. et al.: *Proc. 5th Int. Conf. on Zinc and Zinc Alloy Coated Steel Sheet (Galvatech '01)*. Verlag Stahleisen GmbH, Düsseldorf, 2001, p. 145
- 6) Tanaka, S. et al.: *Proc. 5th Int. Conf. on Zinc and Zinc Alloy Coated Steel Sheet (Galvatech '01)*. Verlag Stahleisen GmbH, Düsseldorf, 2001, p. 153
- 7) Morimoto, Y. et al.: *Tetsu-to-Hagané*. 89, 161 (2003)
- 8) Hisamatsu, Y.: *Namari to Aen (Lead and Zinc)*. 155, 1 (1990)
- 9) Kamio, A.: *J. JILM*. 52, 479 (2002)
- 10) Hillert, M. et al.: *Acta Chem. Scand*. 24, 3618 (1970)
- 11) Liang, P. et al.: *Thermochemica Acta*. 314, 87 (1998)
- 12) Frank, F. D. et al.: *Acta Cryst.* 11, 184 (1958)
- 13) Frank, F. D. et al.: *Acta Cryst.* 12, 483 (1959)
- 14) Ohashi, W.: Ph. D. Thesis, Harvard University, 1989
- 15) Gonzales, F. et al.: *Metall. Mater. Trans.* 37A, 2797 (2006)
- 16) Ohashi, T. et al.: *Tetsu-to-Hagané*. 62, 614 (1976)



Wataru YAMADA
General Manager,
Mathematical Science & Technology Research Lab.
Advanced Technology Research Laboratories
20-1, Shintomi, Futtsu, Chiba 293-8511



Hidetoshi HATANAKA
Manager
Flat Products Technical Dept.
Flat Products Division



Kazuhiko HONDA
Manager, Dr.Eng.
Quality Management Div.
Kimitsu Works



Kohsaku USHIODA
Fellow, Dr.Eng.
Technical Development Bureau



Koki TANAKA
Chief Researcher, Dr.Eng.
Materials Characterization Research Lab.
Advanced Technology Research Laboratories